 SDHM, vol.9, no.3, pp.201-216, 2013

Fringe Projection Assisted Horizontal Impact Testing

D. Schleh[1] **and D. Liu**[1]

Abstract: Understanding the response of composite materials to dynamic loading is necessary for their safe and efficient application to many of the world's engineering designs where stiffness-to-weight ratios are vitally important. In this study, fringe projection was used and evaluated as means to measure the out-of-plane displacement of composite materials from impact loading involving a projectile accelerated horizontally through the use of gas. The capability of providing out-of-plane deformation measurements can largely enrich the investigation of composite materials under horizontal impact which are commonly performed without any measurement other than projectile velocity. The out-of-plane displacement history was subsequently used in an attempt to evaluate the velocity, acceleration and force histories of the impacted composite materials. An impact based bending stiffness could also be obtained for calculating the composites' resistance to impact loading. However, it should be noted that the duration and energy of the impact events to which fringe projection can be applied is not without limits.

Keywords: Fringe projection, horizontal impact, out-of-plane displacement, composites.

1 Introduction

Composites have been and will be continued to be integrated into mobile apparatuses that are used in military and civilian applications. As a consequence, accurate characterization of the materials under a variety of loading conditions has become a pressing endeavor. Since vehicles are one of the primary applications of composite materials, it is reasonable to expect that the loading conditions to which they are subject will be highly dynamic. As the material composing the body of a vehicle, a common loading scenario would include an impact from the out-of-plane direction to the composite surface. This out-of plane impact could occur across a range of loading rates. The behavior of certain composite materials has previously demonstrated a dependence on the loading rate [Weeks and Sun (1988)]. The

[1] MSU, East Lansing, MI, U.S.A.

reaction of composites subject to various rates of out-of-plane loading needs to be carefully considered for the continued integration of composite materials into ever more advanced applications The characterization process of composite materials subject to out-of-plane loadings requires methods for quantifying the composite response. Moiré and fringe methods have been used in static and dynamic applications to collect out-of-plane contour information in vast array of fields including aerospace [Heredia-Ortiz and Patterson (2003); Fleming and Gorton (2000)], health sciences[Takasaki (1970); Breque, Dupre and Bremand (2004)], materials [Gorthi and Rastogi (2010)] and MEMS [Kokidko, Gee, Chou and Chiang (1996)]. They include reflection moiré, shadow moiré, projection moiré, and fringe projection. For this investigation into measuring deformation of composite materials subject to dynamic out-of-plane loadings, fringe projection was used due to the ease through which the method can be applied to specimens of varying geometry in different experimental setups and the availability of processing software [Heredia-Ortiz and Patterson (2005)].

2 Fringe projection

In fringe projection, a grating consisting of parallel straight lines is placed directly in front of a dedicated light source. The dedicated light source then projects the grating lines onto an object of interest. A camera, positioned elsewhere from the dedicated light source, is used to capture images of the grating lines cast on the object of interest during loading. By examining the deviation of the grating lines from the original straight lines, the out-of-plane shape information of the object of interest due to loading can be determined [Creath and Wyant (1992) and Heredia-Ortiz and Patterson (2005)].

In Fig. 1, the contour interval C is the distance between fringes along the viewing axis. Geometric analysis of a fringe projection setup can be used to relate C to the known pitch of the projected fringes p, the angle between the projecting and viewing axes θ, and the fringe spacing on the reference surface$d$ [Creath and Wyant (1992)], as shown in the following equation.

$$C = \frac{p}{\sin\theta} = \frac{d}{\tan\theta} \tag{1}$$

The viewing axis does not necessarily have to be normal to the reference surface, but a normal viewing perspective does make images more readily interpretable [Heredia-Ortiz (2004)] From Eq. 1, it becomes evident that the sensitivity (which increases as values of C decrease) of an experimental setup can be increased by decreasing p through the use of a finer grating or increasing θ Although a value of 90° for θ would theoretically maximize sensitivity, practically this is not an ideal

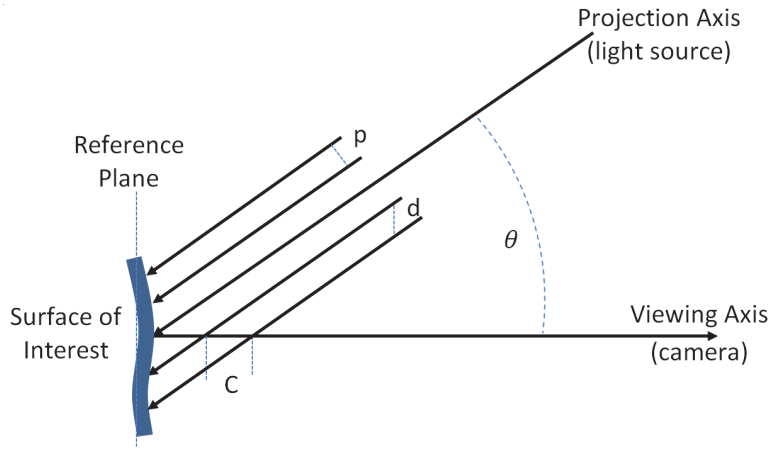

Figure 1: A general depiction of the projected fringes interacting with the surface of interest. The parameters defined are (1)θ, the angle between the projection and viewing axes, (2) p, pitch of projected fringes (3) d, fringe spacing as perceived along the viewing axis and(4) C, contour fringe interval.

choice. A large angle between the viewing and projection axis would cause shadows cast by features on the surface of interest, resulting in regions lacking fringes and the subsequent deformation information. To avoid this, the angle between the projection and viewing axis should not exceed the angles of inclination/declination expected in the deformed surface of interest. There are also practical limitations on the value of the fringe pitch. Theoretically the finer the grating, the higher the sensitivity of the system, but in practice, a low value for the fringe pitch does not equate to an optical setup with increased performance. The projected fringes must be resolvable by the camera used in the optical setup since too fine a grating will result in poor results due to the resolution limits of the camera in capturing images.

3 Processing of images

An automated analysis process was adapted based upon the algorithm resulting from the work by Heredia-Ortiz [Heredia-Ortiz (2004)] and applied through MATLAB. The fringe projection processing algorithms are based upon a phase shifting method and assume an infinite optics experimental setup. The algorithm uses a reference and an object image to infer the deviation of the fringes from a straight line. In the reference image, the fringes are assumed to be vertically oriented. The intensity distribution of vertically oriented fringes is given by

$$I(i,j) = A(i,j)(1+\gamma(i,j)\cos(2\pi f_0 j + \Phi(i,j))) \tag{2}$$

In Eq. 2, A and γ serve as the background illumination and modulation terms, f_0 is the carrier frequency, and Φ represents the phase. Prior to the recent advances in computers and digitization of images, in order to determine depth information, several images of a surface of interest were required with the grating shifted by small, known amounts between images. Currently, this phase shifting can be performed digitally, thus allowing depth information to be extracted from a reference image and a single surface of interest image. Five intensity terms are created through phase shifting of a single image. A phase estimator term Φ^* is generated from the five intensity terms and is proportional to the depth of the surface of interest. By subtracting the phase estimator terms between a surface of interest and a reference surface, changes in surface contour can be determined [Heredia-Ortiz and Patterson (2005)] as follows

$$\Delta z = \frac{\left(\Phi^*_{interst} - \Phi^*_{reference}\right)}{2\pi} * C = \Delta\Phi^* * K \tag{3}$$

From Eqs. 1 and 3, it is clear that C acts as constant proportionality factor. The calibration constant, K in Eq. 3 includes the constants for quantifying Δz for a given optical configuration.

The methodology for calculating contour information described above should also be considered when considering the geometry of a fringe projection setup. The algorithms work well on smooth surfaces with small slopes (less variability in p) when a fine grating is projected (p should be smaller than the features of interest) and when the angle between the projection and viewing axis is small. Values for θ that have produced good results in previous work [Gorthi and Rastogi (2010); Heredia-Ortiz (2005)] were between 10° and 20°.

4 Fringe projection calibration

A calibration procedure is required in the application of fringe projection using the algorithm developed by Heredia-Ortiz [Heredia-Ortiz (2004)]. The calibration procedure serves to identify two primary parameters. The first is to identify the proportionality constant, K, from Eq. 3 The second parameter is a magnification factor that becomes inherent in the optical setup as a result of the infinite optics assumption [Heredia-Ortiz and Patterson (2005)]. The infinite optics assumption was deemed a valid assumption when the distances between the light source and high-speed camera were both an order of magnitude greater than the region of interest. The infinite optics assumption allows for the spacing between fringes on a flat reference surface to be considered constant.

To perform the calibration, firstly, a flat reference surface is placed roughly at the depth from the viewing position that the object of interest would lay. Fringes are

projected onto the reference surface and an image is captured. Secondly, a cone adhered to a flat surface is placed in lieu of the flat reference surface. The diameter and height of the cone are known. The size of the cone should be on the same order of magnitude as the expected height variations in the surface of interest. With respect to impact testing, the cone height should be slightly larger than the expected specimen surface deformation. Fringes are projected onto the cone and an image is captured. The flat reference surface and the cone are then processed through the calibration portion of the fringe projection algorithm to arrive at $K$and the magnification factor for the setup.

An important consideration during the calibration is the frequency of the fringes on the specimen. The accuracy of the fringe projection method is dependent not only on the contour interval of the fringes, but also on the number of pixels used to describe the pitch of the gratings. Gulker [Gulker (2009)] conducted an investigation into the ideal pixel/pitch ratio. The results show the best accuracy in measurements taken with a ratio about 7 pixels/pitch. As the pixels/pitch ratio falls below 7, the accuracy of the fringe projection method decreases more significantly than the accuracy decreases when progressing between 7 and 11 pixels/pitch range.

5 Fringe projection applied to the gas assisted horizontal impactor (GAHI)

The Gas Assisted Horizontal Impactor (GAHI) uses nitrogen gas to propel a projectile horizontally through a guide tube and into a vertically positioned specimen, resulting in out-of-plane deformation of the specimen. The specimen in its fully clamped boundary fixture is housed in a protective steel box with a shatter resistant viewing window. Fringe projection was integrated into the GAHI to measure the out-of-plane displacement during impact from the projectile. The fringes were projected directly onto the non-impacted specimen surface from the light source. The light source consisted of a 1000 watt halogen bulb. A 20 lines/mm Ronchi ruling was placed behind a 12.5-75 mm zoom TV lens. The TV lens was used to focus and adjust the fringe pitch on the specimen surface. To capture images for processing, a Vision Research Phantom v12.1 high-speed camera was used. The camera was outfitted with a Carl Zeiss Planar T* 1.4/85 mm ZF.2 lens. A 254 mm x 254 mm (10” x 10”) mirror was positioned vertically to facilitate high-speed camera viewing of the specimen surface. The mirror was oriented at 45° with respect to the normal of the specimen surface to provide a normal viewing perspective for the high-speed camera.

The GAHI experimental setup is depicted in Fig. 2 and experimental details are contained in Table 1. The distance that the light travels from the specimen to the high-speed camera and from the specimen to the light source was 1270 mm (50”). The angle between the viewing and the projected axis, θ, was 37° The distance

between the light source and the camera was 1016 mm (40”).

For the testing conducted, the desired projectile velocities were varied from 50 m/s to 110 m/s in increments of 15 m/s by adjusting the pressure of the nitrogen gas used to propel the projectile. Prior to the testing, the relation between the gas pressure and the projectile velocity was established with the use of a high-speed camera and a fixed measurement reference which was placed within 25.4 mm (1”) radius of the projectile flight path. The projectile velocity was measured over several centimeters so that an average velocity was taken. It was also measured across the distance that a specimen would have been positioned if an actual test was occurring. Projectile velocities were not measured at the same time at which an impact test was conducted.

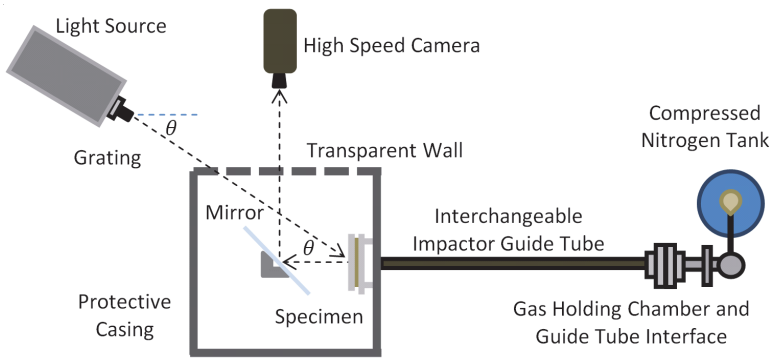

Figure 2: Viewed from above, schematic of the GAHI to which fringe projection was applied.

The GAHI experimental setup requires a balance between optical parameters, physical geometries, and impact durations. For the GAHI geometry, the lower limit of θ is restricted due to the placement of the protective casing surrounding the specimen. The short loading durations necessitate the need for high frame rates, which come at the expense of image resolution and illumination. A point of emphasis during testing was achieving a high testing frame rate with sufficient contrast in the captured images so that deformed fringes were identifiable.

6 Accuracy of fringe projection applied to GAHI

Dimensions of the calibration cone were measured using fringe projection for the configuration depicted in Table 1. From Table 2, the accuracy of the measurements were within 2% for the described configuration. Fringe projection has been re-

Table 1: Experimental details.

Specimen Diameter	127 mm (5")
Specimen Thickness	3.12 mm (0.123")
Impactor Diameter	6.35mm (0.25")
Impactor Mass	4.217 g
Duration of Loading	< 0.10 ms
Test Frame Rate	88,050 fps
Images Captured During Loading	< 8
Test Image Resolution	368 x 144
Test Area of Interest	108 mm x 42 mm
Fringe Pitch on Reference Plane	2.186 mm
Spatial Resolution	3.42 pixels/mm
Calibration Constant	0.46581 mm/rad

ported to be accurate within 1% of the measurement range [Heredia and Patterson (2005)]. Images from the calibration procedure can be seen in Figs 3 and 4.

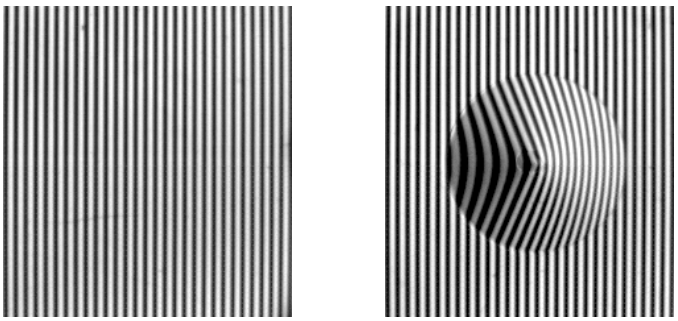

Figure 3: Reference plane and cone images with projected fringes.

7 GAHI test results

Displacement histories of a 6.35mm (0.25") projectile striking 5-ply composite plates at 50, 65, 80, 95, and 110 m/s are featured in Fig. 5. The displacement history corresponding to the initial loading of each specimen was curve-fit using the least-squares curve-fitting technique. The resulting polynomial had to be at least a third-order polynomial as a lesser order polynomial will provide no useful information about the force history. The derivative of the polynomial was then taken to

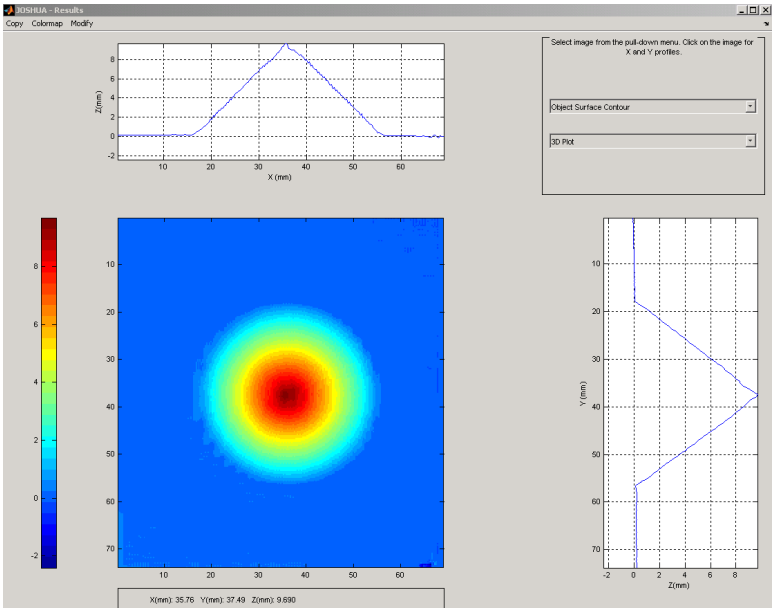

Figure 4: The contour plot showing the results of the calibration procedure with profiles across the peak of the cone.

Table 2: Accuracy measurements and quantification.

	Cone Height (mm)	Cone Radius X-Direction (mm)	Cone Radius Y-Direction (mm)
Established Value	9.81	19.90	19.90
Fringe Projection Measured Value	9.64	20.19	19.62
Percent Difference	1.73	-1.46	1.41

arrive at an expression for the velocity history. An example of a velocity history is presented for the 80 m/s test case in Fig. 6 along with the experimental and curve-fit displacement histories. The second derivative of the curve-fit displacement history function was then evaluated and the result was a function for the acceleration history. The acceleration history for the 80 m/s test case is also featured in Fig. 6. The force history can be obtained by multiplying the acceleration history by the mass of the projectile. It would seem logical that a higher-order polynomial that fits the displacement data very well would be advantageous, but that was not necessarily true for the data sets examined. Evaluating the first and second derivatives

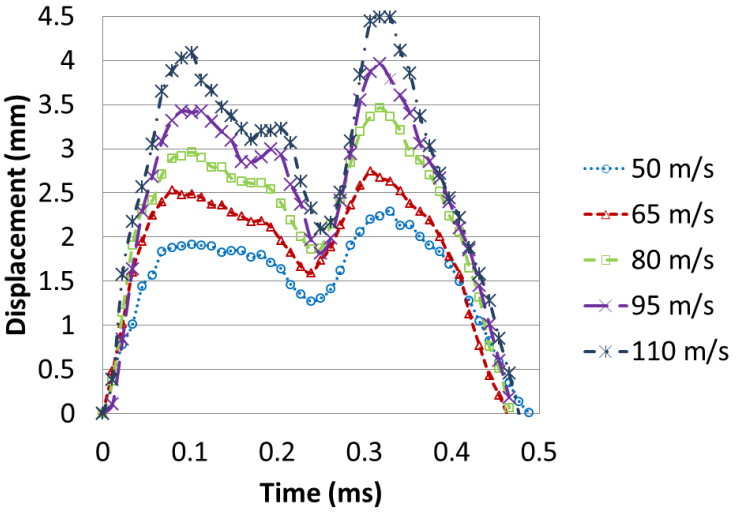

Figure 5: Displacement histories of the impact point from GAHI tests with 5 ply, 127mm (5") specimens made of woven E-glass fibers and a SC-15 matrix.

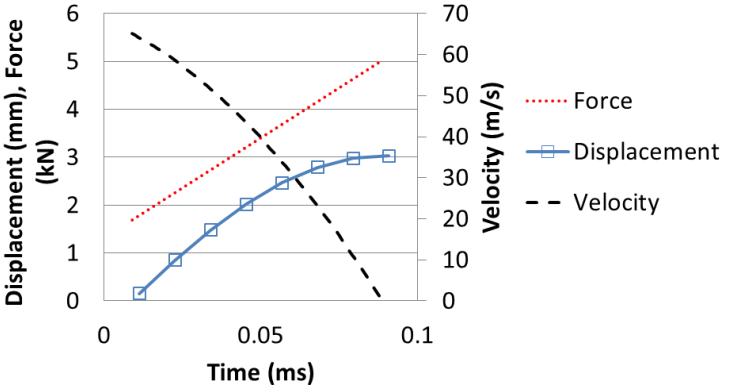

Figure 6: Displacement, velocity and force histories of the 80m/s projectile impact point from fringe projection applied to the GAHI tests with 5-ply, 127mm (5") specimens made of woven E-glass fibers and a SC-15 matrix.

of higher-order polynomials resulted in functions for the acceleration history that did not accurately represent the behaviors of the plate body during testing.

There is a certain amount of error associated with the curve-fitting method. A por-

Table 3: Measured and fringe projection velocities (m/s) from testing on 5 ply, 5" diameter specimens with a 0.25", 4.116g projectile.

Desired Projectile Velocity	50	65	80	95	110
Measured Projectile Velocity	49.58	65.71	80.81	96.71	110.74
Initial Fringe Projection Plate Velocity	32.24	55.19	65.09	74.89	68.51

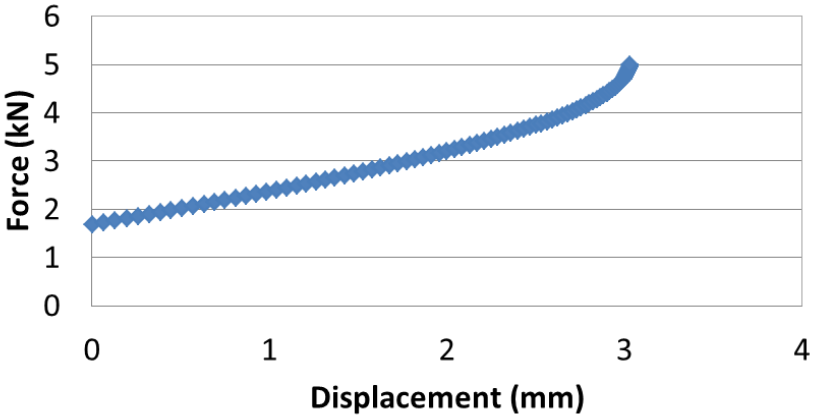

Figure 7: The force-displacement relations regenerated from the curve-fit polynomial of the force and displacement histories in Figure 6.

Table 4: Impact based bending stiffness values at various projectile velocities.

Velocity (m/s)	Impact Based Bending Stiffness (kN/mm)
50	0.875
65	0.359
80	0.745
95	0.434
110	0.651

tion of that error comes from the fact that the exact time at which the projectile first contacts the specimen is not the exact time at which an image is captured with the high-speed camera. The high-speed camera is triggered when nitrogen gas is released from the holding chamber to propel the projectile, recording images of the specimen before and throughout the impact event. Consequently, the amount of deformation occurring before the first data point varies from test to test. This issue is of greater importance with small data sets. The first derivative of the curve-fit displacement history allows for the initial plate velocities to be evaluated. Initial velocities of the plate as measured by fringe projection compared to initial velocities of the projectile are presented in Table 3.

For the graphical determination of the impact based bending stiffness, the curve-fit polynomials and their second derivatives were used to regenerate the displacement and force histories. Errors with curve-fitting such as with the initial displacement point are introduced into the absolute values of the force-displacement relations. The force-displacement relation for the 80 m/s test case of Fig. 5 is included in Fig. 7. Impact based bending stiffness results for all of the test cases of Fig. 5 are presented in Table 4.

8 Double peak investigation

The sample results in Fig. 5 show two distinct displacement peaks from a single projectile striking a composite specimen. To gain insight into the actual physical occurrences, a high-speed camera was used to film the projectile striking the composite plate with the impact conditions the same as those for the 80 m/s test seen in Fig. 5. The Phantom v12.1 high-speed camera was used to record the event at 100,000 fps. The fringe projection video was recorded at 88,050 fps. Testing events were filmed above the frame rate used to capture the fringe projection results because of the lighting restrictions imposed through the application of fringe projection were no longer present.

The double peak can be attributed to the passage of a wave through the plate prior to the composite plate recovering fully from the deformation from the projectile impact. There are two deformation behaviors that are observable in the videos with one (plate body) occurring much more slowly than the other (plate center). As the load is applied at the plate center, the entire composite plate experiences a certain degree of deformation. The plate center experiences the greatest displacement with plate body experiencing an ever decreasing degree of displacement as the distance from the center of the plate increases until the constrained boundaries with zero displacement are reached. This gradual displacement is seen in the observation videos as the relatively gradual bending of the plate body. The plate body as a whole oscillates following impact. Similar to the way a musical drum moves after

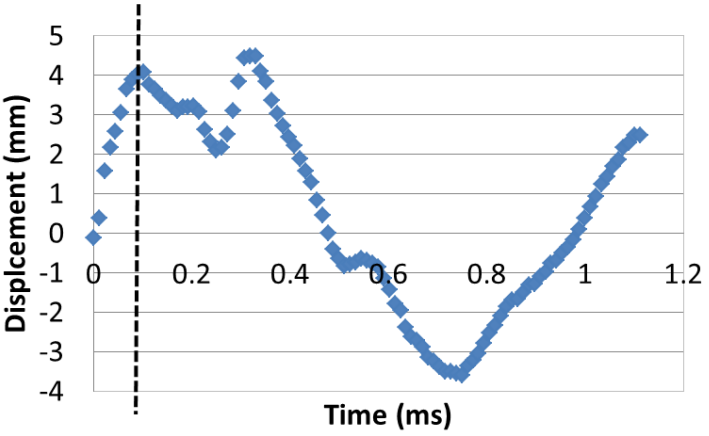

Figure 8: Extended deformation history for the 5-ply, 127mm (5”), 80 m/s test case featured in Figure 5.

being struck. This oscillatory behavior is seen in Fig. 8 as the point of impact experiences a positive displacement (0 to 0.5 ms), a negative displacement (0.5 to 1.0 ms), and a positive displacement (beyond 1.0 ms). Review of fringe projection test video from other tests presented in Fig. 5 can also confirm this behavior of the composite plate following impact.

The second component of the observed displacement occurs much more rapidly. This portion demonstrates itself in the manner in which the plate center seems to deform almost independently of the plate body. This is caused by the waves that propagate outward from the point of impact at the time of impact. These waves travel radially away from the center. The displacement resulting from these waves can be superimposed on to the relatively slow and gradual displacement of the plate body. These waves contribute to the mini-peak, trough and second major peak seen on the displacement history curves near 0.20 ms, 0.25 ms and 0.32 ms, respectively in Fig. 9. The second peak is the result of a wave that had traveled radially outward from the specimen center, been reflected, and had reached the impact point prior to the movement of the plate body from its initial deformed state (0 to 0.5 ms).

9 Discussions

A significant factor to consider in the application of fringe projection to dynamic impacts is the duration of the impact event. The frame rate of the high-speed camera used to record the event is inversely correlated to exposure time. As the frame rate

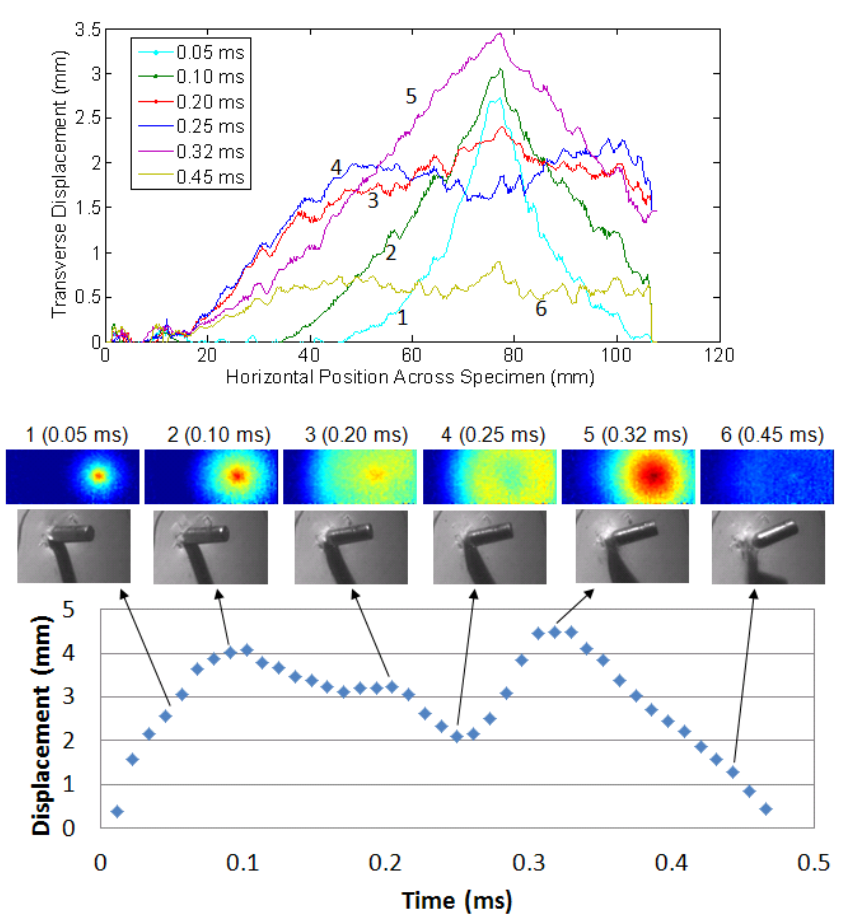

Figure 9: Fringe projection displacement history (bottom) correlated with the high-speed video of the projectile striking the impact surface and the horizontal displacement profiles (top). The case documented is for a 5 ply, 127mm (5") specimen with the projectile striking a composite plate at 80 m/s.

is increased, the exposure time or the time the camera collects light for each image decreases. At some point, the intensity of the light captured by the camera will be insufficient to generate an image with distinguishable features. For dynamic testing this can be problematic as a certain exposure time or frame rate will be required to achieve sufficient data resolution. One solution to this issue is to increase the light intensity and the contrast that exists in the object of which an image is desired. For fringe projection, increasing the lighting in the test setup cannot be achieved by

simply adding additional light directly onto the specimen since applying lighting directly to the specimen will drown out the projected fringes. Increases in lighting must originate from behind the projected grating. The light emitted from behind the grating, must pass through the grating and a focusing lens. The lens is used to focus the fringes on the object of interest and vary the pitch. Light intensity losses are sustained as the light travels through the grating and the focusing lens. Finding the brightest light source possible is recommended for high-speed tests, although it may be problematic due to cost, opportunity or applicability. The light-grating source could also be placed closer to the test specimen so that losses of light intensity are reduced. Performing this action also has its limits in that the closer the light source and camera are to the specimen, the less the idealization that fringe pitch is constant across the area of interest is applicable. Also, restricting this option is that the specimen may be large in size or the camera lens in use has a relevant minimum focusing distance.

From experimental investigations, the upper limit of the frame rates capable of producing processable fringe projection images is in the 120,000 to 130,000 fps range for the equipment used. The accuracy of the data gathered at the upper frame rate should be approached with caution. The application of higher frame rates to large test specimens is also limited by the achievable image resolution (size of the picture). Given that a portion of the specimen fixture (serves as a zero displacement reference) as well as the region of impact needs to be contained in the camera field of view, larger test specimens require greater image resolution. Image resolution and frame rate are inversely correlated, resulting in the use of lower frame rates to accommodate larger test specimens in the application of fringe projection.

10 Summary

Fringe projection is used to measure out-of-plane contour information. In this s-tudy it has been used with the gas assisted horizontal impactor to measure out-of-plane displacement. Fringe projection provides a full-field means through which the out-of plane displacement of composite plates can be measured. The displacement history may be used to calculate the velocity history, acceleration history and force-displacement relations of the impacted materials. This facilitates the study of composites under high and varying rates of loading.

When applying fringe projection, the following parameters need to be carefully considered:

1. the interaction among lighting, frame rate and impact duration
2. the pixel/pitch ratio – The lower limit of the fringe pitch on the specimen

surface will be restricted by the camera used for a given test configuration.

3. the infinite optics assumption – The viewing vs. projecting distances and the specimen size vs. deformation should be considered.

4. the angle between projection and viewing – Angles between 10˚-30˚ have shown reasonable results.

Although fringe projection can be useful means to measure dynamic out-of-plane motion, it is not without its limitations. Severe damage to the non-impact specimen surface is one of them as this corrupts the data. The lighting limitation is another. It stems from the need to project fringes on an object of interest from a significant distance while using a high-speed camera to collect images, resulting in a limit on the impact duration of the dynamic events to which fringe projection should be applied. These limitations require attention when considering application of fringe projection.

Acknowledgement: This research was sponsored by the Army Research Laboratory and was accomplished under Cooperative Agreement Number W911NF-11-2-0017. The authors wish to express their sincere appreciation for the financial support.

References

Breque, C.; Dupre, J. C.; Bremand, F. (2004): Calibration of a system of projection-moiré for relief measuring: biomechanical application. *Optics and Lasers Engineering*, vol. 41, pp. 241–260.

Creath, K.; Wyant, J. (1992): Moiré and Fringe Projection Techniques. *Optical Shop Testing*, 2nd ed., Edited by D. Malacara, Wiley, New York, pp. 653-685.

Fleming, G. A.; Gorton, S. A. (2000): Measurement of rotorcraft blade deformation using Projection Moiré Interferometry. *Journal of Shock and Vibration*, vol. 7, no. 3. pp. 149-165.

Gorthi, S. S.; Rastogi, P. (2010): Fringe Projection Techniques: Whiter we are? *Optics and Lasers Engineering*, vol. 48, no.2, pp. 133-140.

Gulker, B. (2009): *Techniques for Enhancing Impact Testing*, Master's Thesis, East Lansing, MI, Michigan State University.

Heredia-Ortiz, M. (2004): Novel Developments of Moiré Techniques for Industrial Applications Doctoral Thesis, Sheffield, UK, University of Sheffield.

Heredia-Ortiz, M.; Patterson, E. A. (2003): On the Industrial Applications of Moiré and Fringe Projection Techniques. *Strain,* vol. 39, pp. 95-100.

Heredia-Ortiz, M.; Patterson, E. A. (2005): Location and Shape Measurement Using a Portable Fringe Projection System. *Experimental Mechanics*, vol. 45, no. 3, pp. 197-204.

Kokidko, D.; Gee, L.; Chou, S. C.; Chiang, F. P. (1996): Method for measuring transient out of plane-deformation during impact. *International Journal of Impact Engineering,* vol. 19, pp. 127-133.

Takasaki, H. (1970): Moiré Topography. *Applied Optics*, vol. 9, pp. 1467-1472.

Weeks, C. A.; Sun, C. T. (1998): Modeling non-linear rate-dependent behavior in fiber-reinforced composites. *Compos Science Technology*, vol. 58, pp. 603–611.